

**BUKU PROFIL PENYELIDIKAN SKIM GERAN PENYELIDIKAN
FUNDAMENTAL (FRGS) FASA 1/2013 DAN FASA 2/2013**



**A NEW ALGORITHM TO IDENTIFY NONLINEAR VIBRATION OF CAR
BODY IN WHITE (BIW) STRUCTURE**

DR. MOHD. SHAHRIR BIN MOHD. SANI (Project Leader)

DR. MOHD. FAIRUSHAM BIN GHAZALI

MOHAMAD ZAIRI BIN BAHAROM

MOHD. FADHLAN BIN MOHD YUSOF

PROF. DR MD. MUSTAFIZUR BIN RAHMAN

AUTOMOTIVE ENGINEERING CENTRE (AEC),

UNIVERSITI MALAYSIA PAHANG

PEKAN CAMPUS

PAHANG DARULMAKMUR

MECHANICAL ENGINEERING

ABSTRACT (120 words)

In this project, the nonlinear force appropriation identification approach is applied to the detection of nonlinear or piecewise linear stiffness. The methodology will demonstrate using both simulations and experiments by hanging the car body structure with proper elastics bungee cord. The finite element models of the body structures will be built in finite element package and perform model updating to minimise error between experimental and numerical results. Mass and stiffness matrices can be extracted after model updating process. The force appropriation method is implemented to determine the force vector that would excite a single mode of the underlying linear structure a time. At the end of the research, the proposed method is expected to identify nonlinearity of car body structure.

1. INTRODUCTION

Linear identification in structural dynamics is matured and well established [1-3]. Nowadays, nonlinear identification has become a very popular area in structural dynamics. Most of engineering structures exhibit some degree of nonlinearity characteristics especially when the deformations are large [4-5]. Nonlinear systems have a range of behaviour not seen in linear vibrating systems. Furthermore, nonlinear dynamic analysis becomes very important for the identification of damage in structures. Detection, localisation and quantification of nonlinearity are very common in nonlinear structural dynamics area [6-7]. Five typical sources of nonlinearities in structural dynamics were as follows: geometric nonlinearity, inertia nonlinearity, material nonlinearity, damping dissipation and boundary conditions. This research presents the identification of nonlinear body in white structure using combination force appropriation and restoring force method. Test structure in this research represents the configuration body in white (BIW) structure hanged with bungee cord.

2. RESEARCH METHODOLOGY

Research methodology for this project as stated below:

- a) Phase 1:
 - Selection of materials and purchasing equipment for proposed studies
 - Physical measurement and test rig fabrication
- b) Phase 2:
 - Numerical Study
 - Finite Element Modeling
 - Finite Element: Normal Mode Analysis
- c) Phase 3:
 - Experimental Setup
 - Conduct modal test: impact hammer and single shaker
 - Conduct MIMO Normal Mode Test: multi-shaker
- d) Phase 4:
 - Develop algorithm for nonlinear identification
 - Analysis Result

3. LITERATURE REVIEW

There have been many studies on the use of system identification methods to identify structural nonlinearity, which include changes in natural frequencies, mode shapes and damping ratios. Masri and Caughey [8] introduced the restoring forces surface (RFS) to identify nonlinearity in single-degree of freedom (SDOF) systems by exploiting Newton's 2nd law to directly measure restoring and dissipative forces in the system. RFS was extended by [9] to identify multi-degree of freedom (MDOF) systems by transforming the equations of motion from physical to modal coordinate space. RFS is more efficient than the Weiner-kernel approach in identifying nonlinear dynamic systems of the types considered. The parametric identification method by force state mapping technique was developed [10], which is similar to RFS. Dimitriadis and Cooper [11] attempted to identify MDOF systems using a variant of RFS method, which considers time response at similar amplitudes, and subsequently, constant nonlinear restoring forces could be achieved. Kerschen et al. [12] applied RFS method for two different cases: a symmetrical nonlinear beam with piecewise linear stiffness and an asymmetrical nonlinear beam with bilinear stiffness. The nonlinear identification method recently proposed [13-14] is based on the measured linear and nonlinear Frequency Response Functions (FRFs). The method is easy to implement and requires standard testing methods. The data required is limited with measured linear and nonlinear FRFs. A method or procedure for the identification of non-linear single and multi-degree of freedom using restoring forces method with three types of nonlinearity was simulated by [15]. Noel et al. [16] demonstrated that the Restoring Force Surface (RFS) method can provide a reliable identification of a nonlinear spacecraft structure. The nonlinear component comprises an inertia wheel mounted on a support, the motion of which is constrained by eight elastomer plots and mechanical stops. Several adaptations to the RFS method are proposed, which include the elimination of kinematic constraints and the regularization of ill-conditioned inverse problems.

Detection, localization and identification of nonlinearity are very significant in nonlinear structural dynamics area observed that an identification process involved three stages [17-18]: detection, characterisation and parameter estimation as shown in Figure 2.1. Identification of nonlinear systems is an essential part of the verification and validation process. Roache [19] showed that verification is a process where computations in mathematics are performed correctly. On the other hand, validation refers to formulating mathematical model and selecting coefficient to describe the systems.

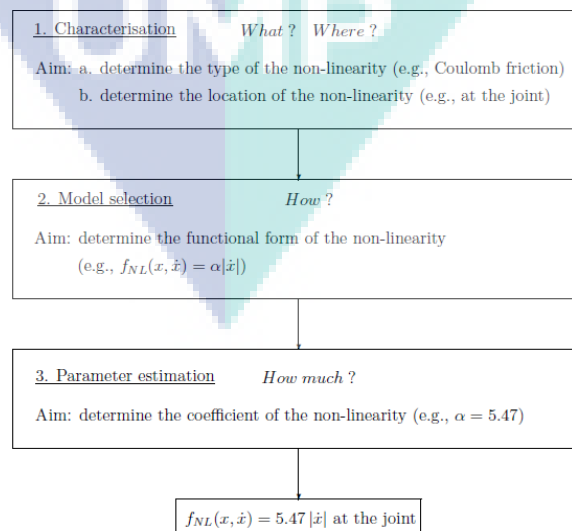


Figure 2.1: Identification Process [18]

There have been many studies on the use of system identification methods to identify structural nonlinearity, which include changes in natural frequencies, mode shapes and damping ratios. Kerschen et al., classified nonlinear identification methods into seven categories: bypassing nonlinearity, linearisation, time domain method, frequency domain method, modal methods, time-frequency analysis, black box modelling and structural model updating [20]. The following is a brief description of the most popular techniques that have been carried out in the last thirty years.

Ibanez seemed to be a pioneer in nonlinear identification research area. Authors obtained dynamic properties such as damping, eigen-frequencies, mode shapes, and nonlinear effects from experimental data [21]. Masri and Caughey introduced the restoring forces surface (RFS) to identify nonlinearity in single-degree of freedom (SDOF) systems by exploiting Newton's 2nd law to directly measure restoring and dissipative forces in the system [22]. This technique expresses the nonlinear component of SDOF systems by measuring three different parameters; displacement (y), velocity (\dot{y}), and time (t). These parameters are plotted with 3D diagram with three axes; restoring forces (RF) versus displacement (y) versus velocity (\dot{y}). Chebyshev polynomials can be used to characterize the resulting surface. The shape of the diagram can reveal the type of nonlinearity such as cubic stiffness, bilinear stiffness, saturation, clearance or backlash, Coulomb friction or nonlinear damping.

RFS was extended by Masri et al. [23] to identify multi-degree of freedom (MDOF) systems by transforming the equations of motion from physical to modal coordinate space. The method can be used with deterministic or random excitation to identify dynamic systems with arbitrary nonlinearities, including those with hysteretic characteristics. Authors claimed that RFS is more efficient than the Weiner-kernel approach in identifying nonlinear dynamic systems of the types considered. The parametric identification method by force state mapping technique was developed by Crawley and Aubert [24], which is similar to RFS. They carried out experiments to demonstrate the technique and the results showed strong structural nonlinearities, which were cubic hardening spring, friction, and impact phenomena. In addition, Dimitriadis and Cooper attempted to identify MDOF systems using a variant of RFS method, which considers time response at similar amplitudes, and subsequently, constant nonlinear restoring forces could be achieved [25]. This approach allows the identification of small systems with the least-squares method. Nevertheless, there is a limitation to large systems that requires the try-and-error method to detect the location of nonlinearity. Kerschen et al. applied RFS method for two different cases: a symmetrical nonlinear beam with piecewise linear stiffness and an asymmetrical nonlinear beam with bilinear stiffness [26]. The polynomial model identifies a significant cubic stiffness with mean square error (MSE) of 1.70% and the non-polynomial model achieved an MSE of 1.80%. It shows that both models gave similar results. For bilinear stiffness, the authors concluded that reliable identification has been achieved with similar MSE and good fitting of restoring forces.

Simon and Tomlinson used the Hilbert transform (HT) method to identify linear and nonlinearity of structures in frequency domain [27]. The HT approach has been shown to be a suitable tool to identify nonlinearity and it has the capacity to quantify nonlinearity, subject to the input excitation being sinusoidal. Tomlinson described the development in the use and application of HT for identifying and quantifying nonlinearity using simulated and experimental FRF. Calculation of HTs was carried out in the time domain employing the fast Fourier transform (FFT) procedures and new correction terms were proposed. Linearisation with HT and random excitation methods

were applied to experimental data to reveal similar trends in the extracted modal parameters [28].

Feldman proposed a new method for analysing and identifying nonlinear vibration of structures by considering the primary and higher harmonics of the solution [29]. The method is based on two other HT methods: the method for extracting instantaneous frequency and Hilbert Vibration Decomposition (HVD) method that splits non-stationary wideband oscillating signal into separate components. Instantaneous modal parameters from nonlinear systems are oscillating functions due to divergences from a linear relationship between specific input and output of the system. These nonlinear distortions are characterised by the appearance in the output of a system of frequencies, which are linear combinations of the fundamental frequencies and all the high harmonics present in the signals. Furthermore, HVD considers the high super harmonics, which are more precise identification of nonlinear systems, including nonlinear elastic and damping force characteristics.

Reverse path (RP) method allows proper estimate of frequency response functions (FRF) and distributed nonlinearity coefficients. Bendat introduced the RP method and was followed by Rice and Fitzpatrick who used this method for MDOF systems [30-31]. Nevertheless, this method requires external force to be applied at the location of nonlinearity.

In addition, reverse path spectral approach was studied by Richard and Singh [32] for identifying nonlinear systems using Gaussian random excitation. They developed the technique for the underlying linear systems without contaminating effects from the nonlinearities. The authors estimated the conditioned FRF and identified nonlinearities by estimating the coefficients of analytical functions. This method was successfully simulated in several systems: a three-degree-of-freedom system with an asymmetric nonlinearity, a three-degree of freedom system with distributed nonlinearities and a five-degree-of-freedom system with multiple nonlinearities and multiple excitations. Marchesiello extended this method to conditioned reverse path (CRP) to separate nonlinear part of the equation of motion from the linear part and construct the ranking of uncorrelated response part in the frequency domain [33]. The author claimed that CRP was very straightforward to identify nonlinearity for MDOF system using random excitation. However, some refinement is needed to improve the discrimination performance and to reduce analyst interaction.

Lin et al. proposed an extension of the method to detect nonlinearity from analysis of complex modes. For SDOF systems, two complex nonlinear equations are built by considering two points of equal magnitude before and after resonance [34]. They also considered MDOF systems and successfully solved a numerical case for a two-degree of freedom system. However, Siller tried a similar approach, but concluded that the method only applied to systems with friction damping or weak stiffness nonlinearity. He explained further that for strong cubic stiffness systems, it is impossible to locate a point of similar magnitude after resonance [35].

Slaats et al. put forward three mode types: tangent modes, modal derivatives and static modes for reducing nonlinear dynamical from finite element discretisation [36]. Tangent modes are acquired from an eigenvalue analysis with a tangent stiffness matrix where modal derivatives (second order terms) with respect to modal coordinates containing the reduction information. However, integration of nonlinear dynamic system was reduced by a set of tangent modes, which would contribute to poor results of large displacement. Static modes can be obtained by an incremental Newton-Raphson iteration rule, which ignores the inertia terms. In this paper, positive influence on

computational time was highlighted for nonlinear dynamic reduction technique by numerical examples.

Shaw and Pierre developed a systematic approach to identify only weak nonlinear and continuous systems using nonlinear normal modes (NNMs) [37]. This method conserves the physical nature of nonlinear mode shapes and modal dynamics parameter. By using asymptotic series expansions and transformation, the authors demonstrated how an approximate nonlinear superposition could be employed to rebuild the overall motion from individual nonlinear modal dynamics. Subsequently, Boivin et al. introduced some modifications to this method, which allows performing a legitimate modal analysis from free response of nonlinear systems [38]. They discovered some desirable properties for the modal analysis of linear system based on geometric approach. This methodology ignores the modelled modes invariant from non-modelled ones to reduce the set of equations. Pesheck et.al investigated the multimode invariant manifold method to generate reduced order models for MDOF nonlinear vibration systems [39]. This method is useful for modelling complex structure responses and is important when internal resonances are present between the modes.

An identification of weak nonlinearity of structure has been developed by Rice using the first order function of cubic stiffness nonlinearity [40]. The author described an approach where underlying nonlinear differential equation governing the system is identified. This approach receives the input data in time domain with different levels of excitation and builds the variations of stiffness and damping ratios. A mounted commercial aircraft trim panel was tested to demonstrate this technique.

Soize and Le Fur presented an identification formula based on a stochastic linearization method with random coefficients [41]. The model was defined as a multidimensional linear second-order dynamic system with random coefficients. Furthermore, an optimisation technique was developed to identify the parameters of the probability law of random coefficients. However, the authors concluded that this method could be improved by introducing some statistical dependence between the components of the random coefficients expressed in the modal coordinates in order to model the coupling of the eigenvectors induced by the weak nonlinearities.

Rosa et al. developed an optimization approach to estimate the modal parameters of nonlinear systems using goal programming [42]. This method is performed in the frequency domain in order to minimise the total squared error between experimental and estimated values of nonlinear FRFs. Its main purpose was to obtain better accuracy than classical methods in complex cases: highly damped systems, systems of high modal density and noisy experimental data. The results from this goal programming were compared with those obtained from a classical estimation method, the orthogonal polynomials method. They found that this algorithm could produce high-accuracy results even when using poor initial estimates.

The force-state mapping technique for nonlinear systems was developed by Al-Hadid and Wright [43]. They simplified the identification procedure by Masri and Caughey [22] in order to identify nonlinearity for SDOF and MDOF systems. In addition, the authors used a simple methodology, faster and more accurate for identifying the type and location of discrete nonlinear elements in a lumped-parameter system.

McEwan et al. proposed a method for modelling large-deflection beams using a combined modal or finite element analysis of dynamic response [44]. They developed a special code to construct static nonlinear test cases subjected to prescribed modal forces and resultant modal displacements. Then, regression analysis is applied in order to extract the nonlinear stiffness coefficients. The beam problem can then be solved for

any force-time history in the reduced degree of freedom modal system. Singular value decomposition (SVD) is required for finding the pseudo-inverse of a rectangular matrix and solving systems that are suspected to be ill-conditioned.

Siller presented two methods: direct path and hybrid modal techniques (HMT) in order to identify nonlinearity from FRF as the input data [35]. The direct path method is a technique to manipulate physical coefficients stored in system matrices. The author stated that optimisation of this method was validated against real measurement and it was found that the nonlinear characteristic was predicted with good accuracy. HMT is similar to a nonlinear superposition technique, in which the underlying linear system is expressed in generalized modal coordinates, while the nonlinearities are kept in the physical domain. The function of the hybrid coordinates is a significant feature to localize the nonlinearities of the system. The author also introduced fast approximation technique (FAT) to allow analytical derivation via newly developed expressions, which establish a link with other nonlinear methods and standard modal analysis techniques.

The auto regressive moving average with exogenous inputs (ARMA) model is one of the popular identification methods in time domain. Based on ARMA, Leontaritis and Billings proposed the nonlinear auto-regressive moving average with exogenous inputs (NARMAX) model [45]. This model works on discrete time and is a nonlinear version of the discrete time ARMA model used in a number of linear methods. It allows the estimation of higher order FRFs by harmonic probing (Billings et al., 1989). Basically, most of the works carried out using this model were based on single input/output data, and it looks most suited to relatively low order complex nonlinear systems. This model does not lend itself simply to acquire a significant physical parametric model and large order multi input-multi output (MIMO) systems that would lead to a massive number of terms. Nevertheless, Thouverez and Jezequel attempted to identify a modal space model using NARMAX by reducing the model order and catering for larger systems [46]. Billings et al. applied orthogonal estimator in order to improve model selection and parameter estimation methods in NARMAX model [47]. Genetic algorithms approach in NARMAX model was successfully developed by Chen et al. [48].

4. FINDINGS

4.1 Introduction

In this section, the results obtained through finite element analysis and experimental modal analysis is shown and discussed. Firstly, the findings of the frequency analysis in finite element of the BIW structure with and without joints modelling strategy is presented. Next, are the results obtained through experimental works using several different settings are shown. After that, correlation of those data before and after performing model updating procedure is presented.

4.2 Finite Element Analysis of BIW Structure

4.2.1 Finite Element Analysis of BIW Model without Joint Modelling Strategies

Although the real BIW structure consists of numerous of joint components such as bolted and welded joints, the initial model of the BIW structure does not include any strategies for modelling the available joint components. The intention is to observe whether the prediction data obtained from a simplified modelling of the BIW structure have an acceptable correlation to the experimental data that are acknowledged as the actual data for the BIW.

Table **Error! No text of specified style in document..1** shows the value of the first five natural frequencies obtained through finite element analysis carried out using SOL 103 in MSC.Nastran/Patran software. The type of vibrational mode for each of the natural frequencies is stated in the table as well. The type of vibrational mode, which indicates whether the structure is subjected to bending or torsional mode is stated by referring to Figure **Error! No text of specified style in document..1** to Figure **Error! No text of specified style in document..5**.

Table **Error! No text of specified style in document..1** Finite element natural frequencies of BIW model without joint modelling

Mode	Natural frequencies (Hz)
1	29.37
2	41.30
3	52.55
4	67.15
5	74.59

In the first mode, the BIW structure is subjected to bending deformation at floor and body side area while roof area was subjected to a combination of bending and torsional deformation as shown in Figure **Error! No text of specified style in document..1**. In the second mode, the structure undergoes second bending motion throughout roof and floor area as shown in Figure **Error! No text of specified style in document..2**. In the third mode, as exhibited in Figure **Error! No text of specified style in document..3**, the different area on the structure experiences bending translation. In Figure **Error! No text of specified style in document..4**, which shows the fourth mode, the body side, roof and floor area undergo bending motion while the front structure area undergoes torsional motion. In the fifth mode as displayed in Figure **Error! No text of specified style in document..5**, the structure undergoes bending deformation at body side and roof area, while the front structure and floor area undergo torsional deformation.

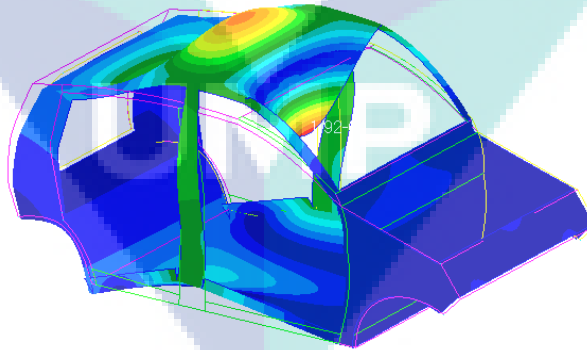


Figure **Error! No text of specified style in document..1** First FEA mode shape at 29.37 Hz

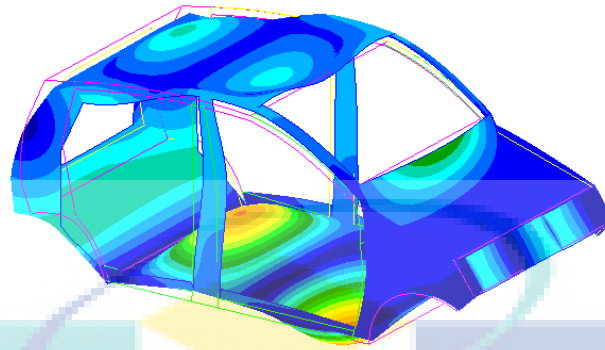


Figure Error! No text of specified style in document..2 Second FEA mode shape at 41.30 Hz

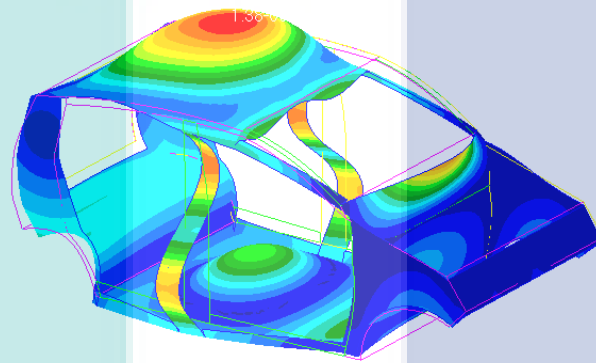


Figure Error! No text of specified style in document..3 Third FEA mode shape at 52.55 Hz

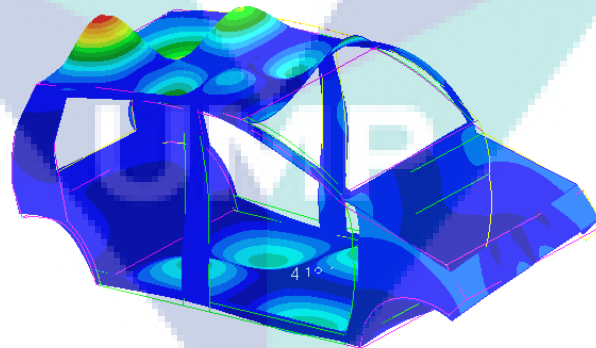


Figure Error! No text of specified style in document..4 Fourth FEA mode shape at 67.15 Hz

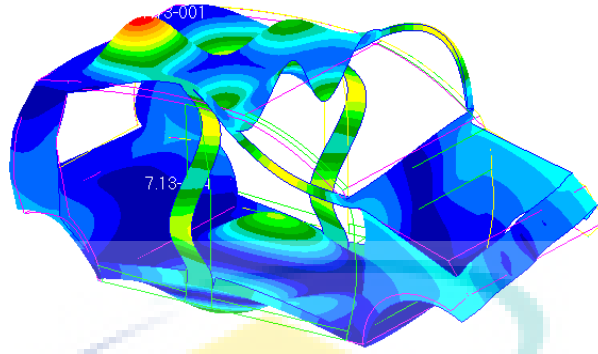


Figure Error! No text of specified style in document..5 Fifth FEA mode shape at 74.59 Hz

4.2.2 Finite Element Analysis of BIW model with different joint modelling approaches

The finite element analysis of the BIW model is broadened to be performed on BIW model that includes the modelling of joint components. In this case, the first approach of modelling the joint components are by using CBAR elements as the connector, while the second approach is using CELAS elements as the connector. The same analysis of SOL 103 is carried out on both BIW model. In order to enact the rigidity of the joint components, CBAR elements are assigned with high value of Young's modulus, and CELAS elements are assigned with immense value of spring constant.

In Table Error! No text of specified style in document..2, the value of natural frequencies of BIW model that uses different approaches of joint modelling are displayed. The value of natural frequencies of the BIW model without joint elements as described in previous section are included in the table as well for comparison purpose.

Table Error! No text of specified style in document..2 Finite element natural frequencies of BIW model using different approaches of joint modelling elements

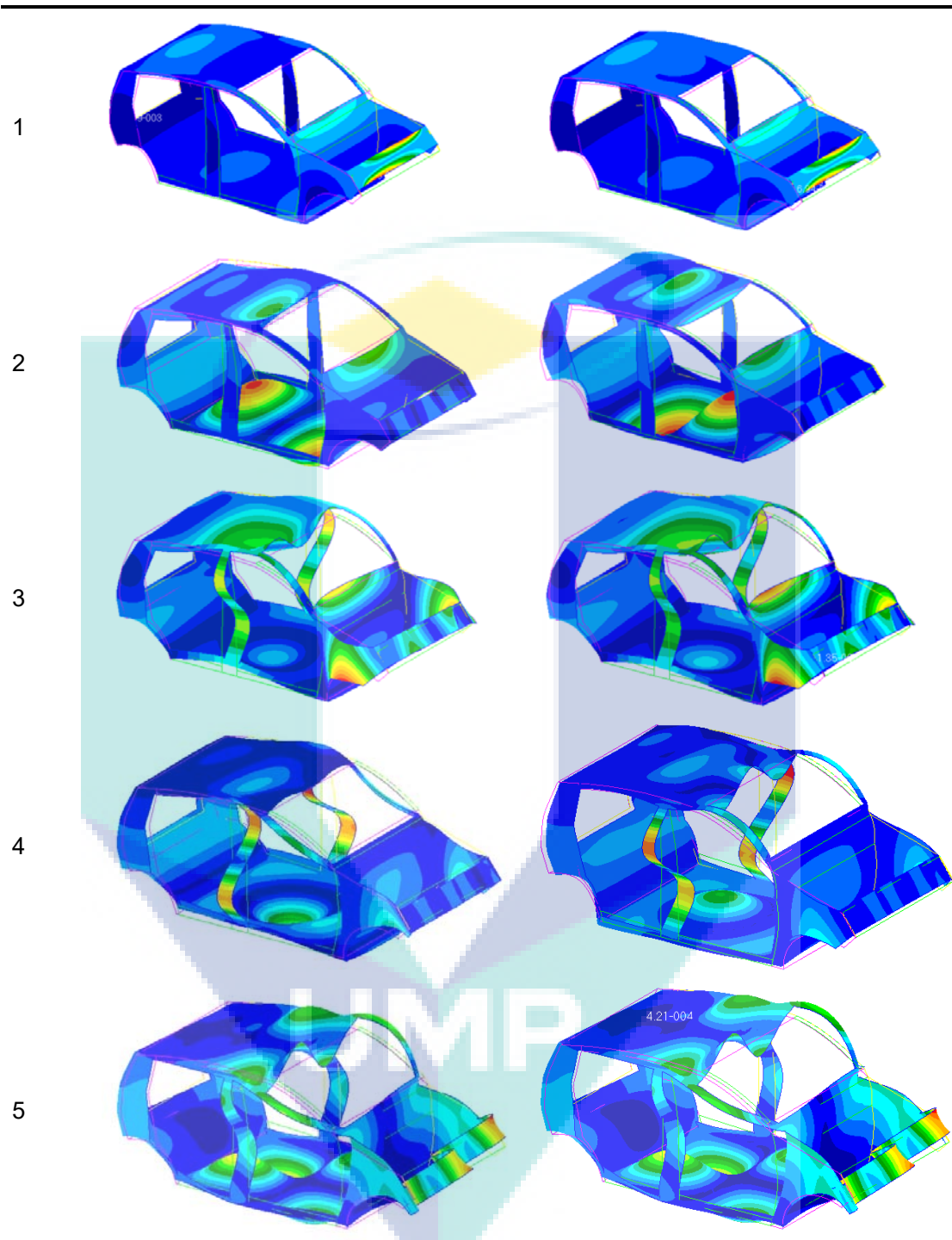
Mode	Natural frequencies (Hz)		
	CBAR	CELAS	Without joint elements
1	29.29	29.30	29.37
2	43.22	43.27	41.30
3	55.70	55.91	52.55
4	62.14	62.41	67.15
5	69.35	69.48	74.59

Meanwhile,

Table Error! No text of specified style in document..3 displays the finite element mode shapes of BIW model that uses CBAR and CELAS as its joint element. As shown in the table, the mode shapes show similar pattern of deformation even though the direction of translation differ from each other visually.

Table Error! No text of specified style in document..3 Finite element mode shapes of BIW model using different approaches of joint modelling elements

Mode	Mode shapes	
	CBAR	CELAS



4.3 Experimental Modal Analysis of the BIW Structure

When conducting impact hammer test, the concerns on the excitation process is one of the important things. The first issue is about pre-trigger delay which without considering to include this step, some input frequency spectrum distortion which will have an effect on the computed FRF. Another issue in impact testing problem is the double hit during the impact. The double hit generally causes a non-uniform and non-flat input spectrum which cause undesirable ripple in in the spectrum. Figure Error! **No text of specified**

style in document..6 show the input time pulse of the impact hammer during the impact testing. As seen on the figure, the signal shows specified single pulse with specified pre-trigger. Therefore, there are no double hit and pre-trigger delay issue when conducting the impact test. In addition, there was no undesirable ripple on the frequency spectrum which signify that the excitation input was done properly.

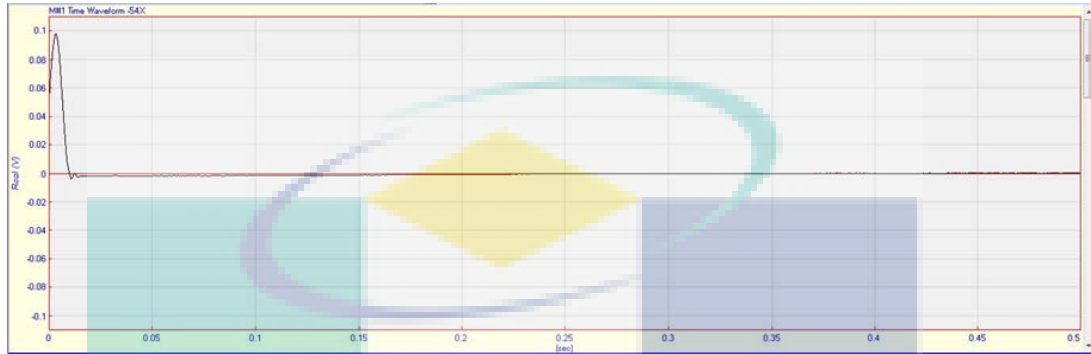


Figure **Error! No text of specified style in document..6** Impact hammer time pulse graph

4.3.1 Data Acquisition Using 1 Tri-axial Accelerometer

Experimental modal analysis is performed on the BIW structure by carrying out impact hammer test on the structure. To ensure the accuracy of the measured experimental results, several factors related to experiments are given serious view and consideration before measuring the modal properties of the BIW structure through impact hammer test. Among the concerned factors are the number of accelerometers employed, number and location of the measuring points, method of support, hanging alignment, and location and method of excitation. In this case, as the accelerometers are lightweight, there are no any mass loading issues when it comes to the arrangement of accelerometers during each experiment since the BIW structure has immense weight. Impact hammer test was made by using two different approaches which are the roving accelerometer method and roving hammer method. For each method, the impact hammer test was carried out twice. Figure **Error! No text of specified style in document..7** and Figure **Error! No text of specified style in document..8** shows the superimposed FRFs based on the 61 measurement points using roving accelerometer method. The available mode indication function in the pre-processing software (ME'scope VES) is used to count peaks from the FRF graph. Mode indicators are useful to estimate the effective number of modes in the frequency range of interest and to determine appropriated force vectors to isolate undamped normal modes of structure. The mode indicator functions (MIF) shows the natural frequencies of the structure. MIFs are defined by the eigenvalues of these matrix products, plotted against frequency. Usually, the existence of a mode of vibration is indicated by distinct peaks in the MIF plot. The range of frequency of interest is set from 0 to 100 Hz.

Peak 1

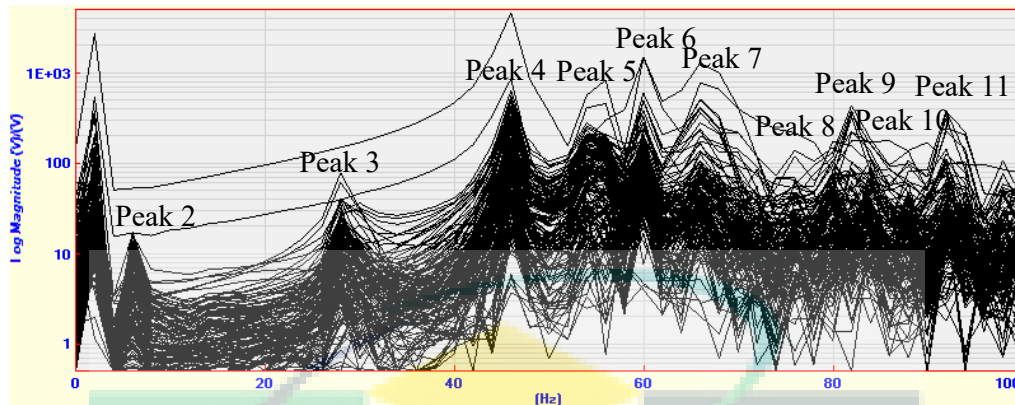


Figure Error! No text of specified style in document..7 Overlaid X, Y, and Z direction traces of FRF using roving accelerometer method with 1 tri-axial accelerometer (Test 1)

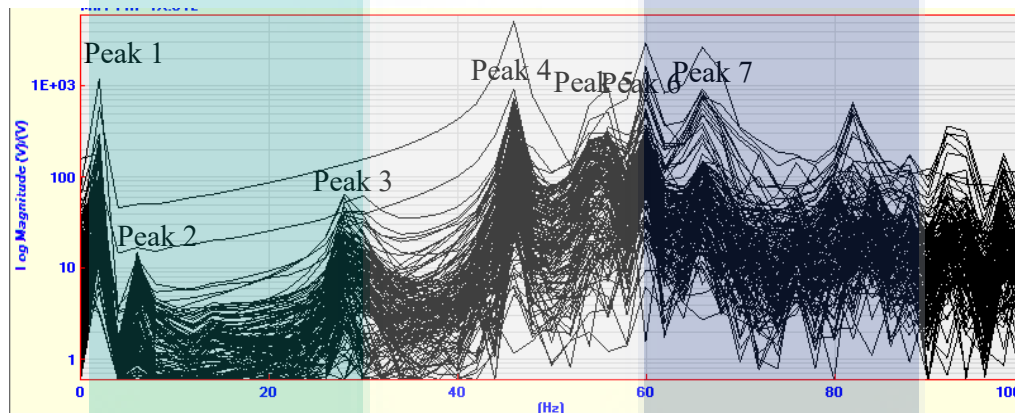


Figure Error! No text of specified style in document..8 Overlaid X, Y, and Z direction traces of FRF using roving accelerometer method with 1 tri-axial accelerometer (Test 2)

The FRF graphs in Figure Error! No text of specified style in document..7 and Figure Error! No text of specified style in document..8, which are obtained through the same method, show almost the same shape and location of the peaks. According to both figures, peak 1 and peak 2 are closely spaced and lightly damped. Thus, MDOF fit is used for curve fitting process. Peak 3 and peak 4 are well separated and lightly damped, so SDOF fit is employed. Peak 5 and upcoming peaks are heavily damped compared to the earlier peaks. Some of the peaks are well separated and some of the peaks are closely spaced. Therefore, the usage of MDOF fit is employed at first but the outcome is still compared to the outcome obtained when using SDOF fit. However, while determining the available mode from the computed FRFs using the MIF indicator available in the software, peak 1 and 2 in the FRF graphs are not indicated as one of the modes. In addition, the value of natural frequencies shown by the first and second peak is relatively small and shows different numerical value for natural frequencies in first and second test. In addition, the experimental model showed free translation and rotation without undergoing any significant internal deformation at all when the mode shape was simulated on those peaks which associate the peaks with rigid body mode. Therefore, the first vibrational mode of the BIW structure is indicated by the peak 3, the second mode is the peak 4 and so on. In the case of close peaks such as peak 6 and peak 7, those peaks are curve fitted into one single mode as both peak simulated similar mode shapes. Therefore, those peaks are considered as close mode.

Meanwhile, in Figure Error! No text of specified style in document..9 and Figure Error! No text of specified style in document..10, the superimposed FRFs obtained using roving hammer method is displayed. Although both tests are carried out using the same measurement point and tri-axial accelerometer, the FRF graph in the second test is noisier and the available peaks look less clear compared to the FRF graph shown in the first test. While using roving hammer method, the response from all directions and locations as gathered through roving accelerometer method cannot be done. This is due to the location of the accelerometer failed to receive excitation from certain point on the BIW structure. Therefore, the response obtained is not as stable as shown in FRF graph obtained through roving accelerometer method.

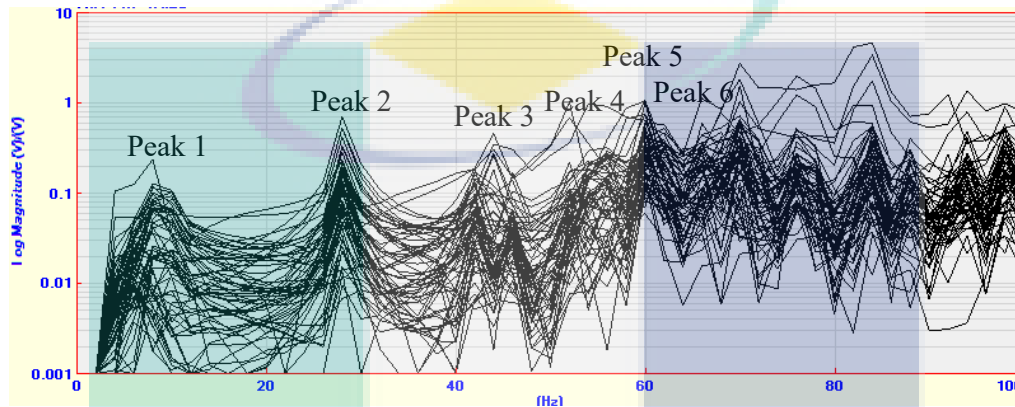


Figure Error! No text of specified style in document..9 Overlaid X, Y, and Z direction traces of FRF using roving hammer method with 1 accelerometer (Test 1)

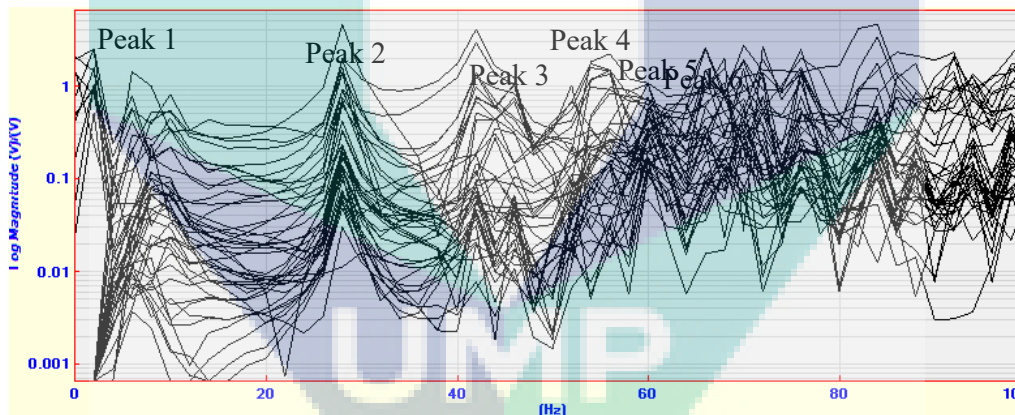


Figure Error! No text of specified style in document..10 Overlaid X, Y, and Z direction traces of FRF using roving hammer method with 1 accelerometer (Test 2)

Although the peaks shown from 50 Hz and above is less clear than the peaks shown below 50 Hz, the curve fitting process has proceeded with the aid of available MIF indicator. Similar to the response obtained through roving accelerometer method, peak 1 in both FRF graphs are not considered as mode as it was not indicated by the MIF and the location of peaks are different in each test. Furthermore, the behaviour of rigid body mode was detected when simulating the mode shape. SDOF fit is used for the peak 2 to obtain the natural frequency of the first mode and MDOF fit is used for the next available peak.

The coherence data for each test is as shown in Figure Error! No text of specified style in document..11. The obtained data were well coherent for the frequency range up until 200Hz. Imperfect coherence results were obtained as the frequency range goes higher because the hammer tips that were used during testing are less feasible to

obtain better signal at high frequency. As the results are mainly focused on lower frequency range, the imperfect coherence results that has been shown for higher frequency value were ignored.

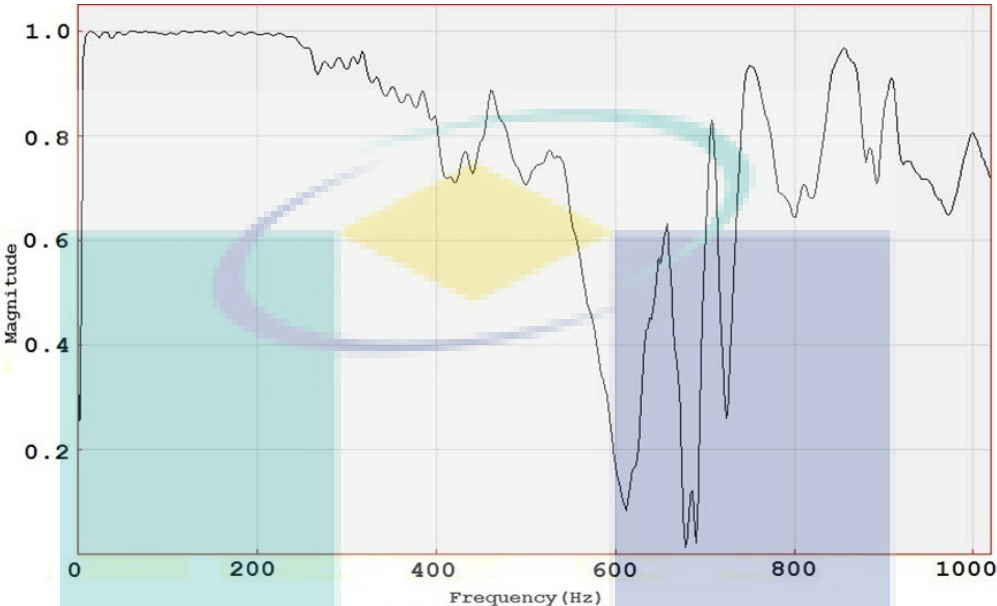


Figure Error! No text of specified style in document..11 Coherence data for FRF when using 1 accelerometer

The value of the natural frequencies of the BIW structure obtained through curve fitting process in all test while using 1 tri-axial accelerometer is compiled and tabulated as shown in

Table Error! No text of specified style in document..4. According to the table, the measurement of the natural frequencies obtained while using roving accelerometer method is more stable than using roving hammer method. Even so, the average for all readings is calculated for the purpose of correlation with the results from other experimental approach.

Although roving accelerometer and roving hammer are considered as two different approaches of conducting the impact hammer test, there is actually no difference between those two tests when it comes to providing the measurements during experiments. Based on the discussion provided by Schwarz et al. regarding the experimental modal analysis, the only difference between those two methods are its experimental configuration and the way responses are recorded into FRF matrices which only affect the generation of mode shapes in certain modes (Schwarz & Richardson, 1999). In addition, Schedlinski et al. provided the comparison of different measurement scenarios in experimental modal analysis. Different test procedure such as impact hammer and shaker test as well as roving accelerometer and roving hammer are carried out and the tests results are evaluated (Schedlinski et al., 2014). Based on this study, there are no significant differences between roving hammer and roving accelerometer. Therefore, taking the average reading can be considered as practical.

Table Error! No text of specified style in document..4 Experimental natural frequencies of BIW structure when using 1 accelerometer

Mode	Natural frequencies (Hz)				Average
	Roving accelerometer		Roving hammer		
	Reading 1	Reading 2	Reading 1	Reading 2	

1	28.4	28.4	28.4	28.8	28.5
2	42.4	42.4	44.4	45.6	43.7
3	55.1	57.9	59.3	55.1	56.9
4	66.4	67.4	69.1	68.8	67.9
5	76.3	76.4	75.6	71.9	75.05

4.3.2 Data Acquisition Using 3 Tri-axial Accelerometers

The next approach of conducting impact hammer test is by using 3 tri-axial accelerometers simultaneously while measuring response on BIW structure. Similar to the previous approach, two different methods of conducting impact hammer test, which is the roving accelerometer and roving hammer method, are employed while using 3 sensors. For each method, the impact hammer test was carried out twice.

Figure Error! No text of specified style in document..12 and Figure Error! No text of specified style in document..13 show the FRF measured using the roving accelerometer method for the first and the second test respectively. As seen in both figures, the location of peaks that indicate the modes of the structure shows no huge difference when compared to the FRF obtained previously while using 1 accelerometer. Peak 1 in both figures, similar to previous test, is not indicated as mode by MIF indicator and showing the characteristic of rigid body mode. Therefore, the first mode of the structure is indicated by peak 2 and SDOF fit is used for curve fitting process. Peak 3 and peak 4 is considered as closed mode as the peaks are closely spaced. Thus, MDOF fit is employed on those peaks. The same case is applied to the next peaks as they are considered as closely spaced.

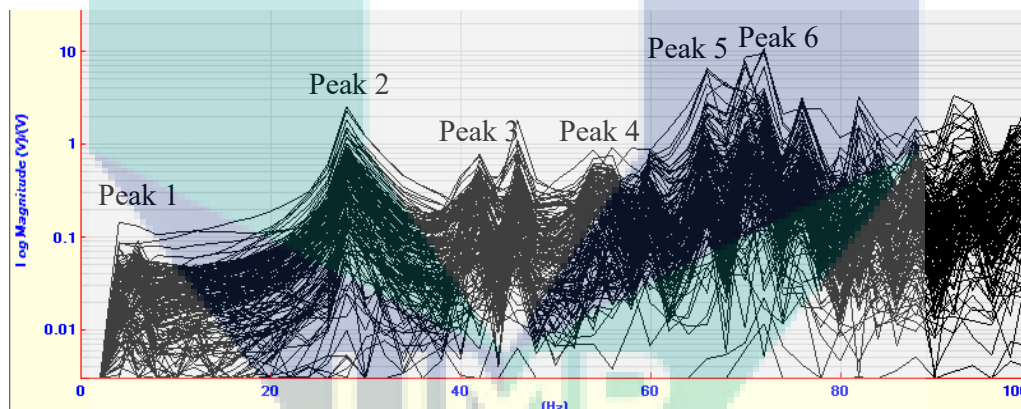


Figure Error! No text of specified style in document..12 Overlaid X, Y, and Z direction traces of FRF using roving accelerometer method with 3 tri-axial accelerometer (Test 1)

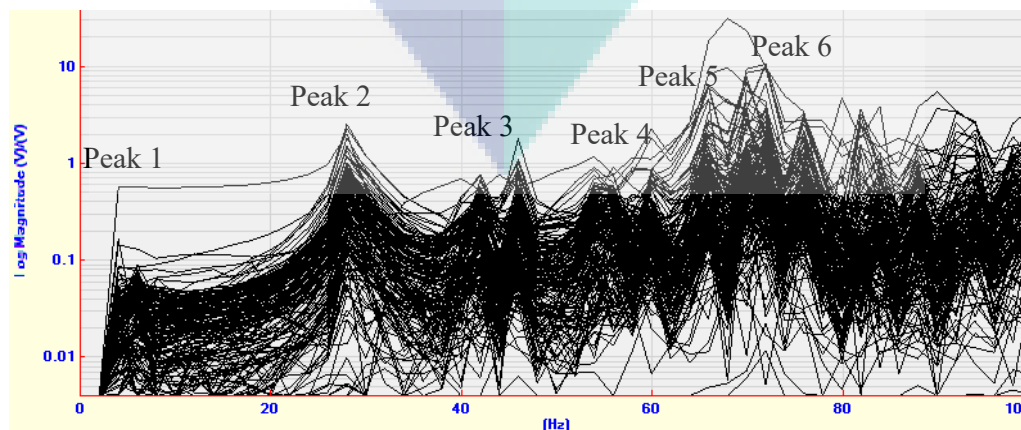


Figure Error! No text of specified style in document..13 Overlaid X, Y, and Z direction traces of FRF using roving accelerometer method with 3 tri-axial accelerometer (Test 2)

Figure Error! No text of specified style in document..14 and Figure Error! No text of specified style in document..15 show the FRF obtained using the roving hammer method for the first and the second test respectively. Based on the figures, although the same method of roving hammer is used, the response obtained when using 3 accelerometers in the test is more stable than using only 1 accelerometer. In addition, the location of peaks that indicates the modes of structures is less different when compared with the FRF obtained in all previous tests. Similar to all previous cases, peak 1 is not considered as the first mode. Moreover, the numerical values for natural frequencies shown by the first peaks in all FRF graph are clearly different each time curve fitting process is carried out. This indicates that the mode shown by the first peak is not stable unlike all other consistent peak, and cannot be considered as one of the vibrational mode of the structure. In addition, there are no vibrational deformation when simulating the mode shape but rather the experimental model showed the movement that indicate the rigid body mode. For curve fitting process, SDOF fit is used for the second peak. MDOF fit is used on the third and fourth peak, fifth and sixth peak, and so on as those peaks are closely spaced. For the peaks that are close to each other, those peaks are considered as one mode as similar mode shapes are simulated.

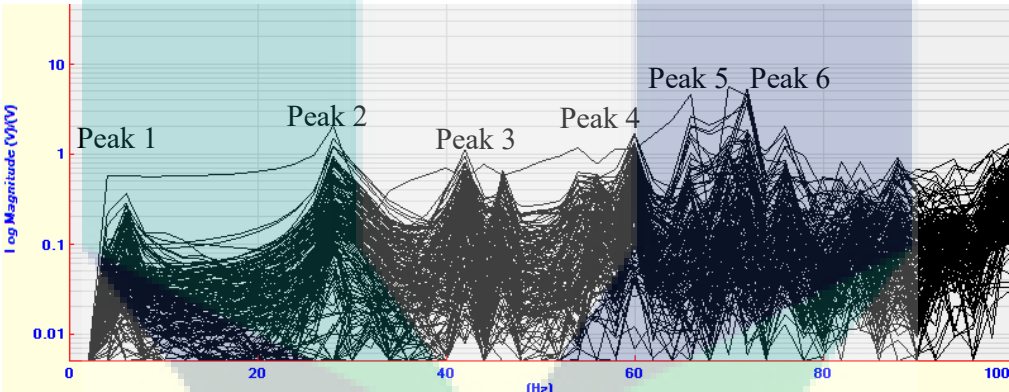


Figure Error! No text of specified style in document..14 Overlaid X, Y, and Z direction traces of FRF using roving hammer method with 3 tri-axial accelerometer (Test 1)

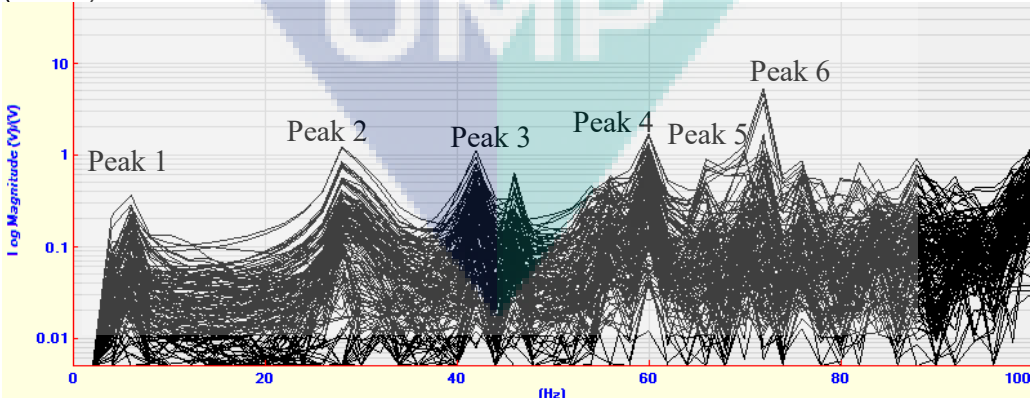


Figure Error! No text of specified style in document..15 Overlaid X, Y, and Z direction traces of FRF using roving hammer method with 3 tri-axial accelerometer (Test 2)

The coherence data for each test is as shown in Figure Error! No text of specified style in document..11. Similar to previous case when using 1 tri-axial accelerometer, the obtained data were well coherent for the frequency range up until 200Hz. The signal then was not very coherent as the frequency range goes higher as the hammer tips used is less suitable for obtaining good high frequency ready. In comparison, the coherence data was better and shows smooth curve up until 100 Hz of frequency range which signify better signal was acquired when employing 3 accelerometers during test.

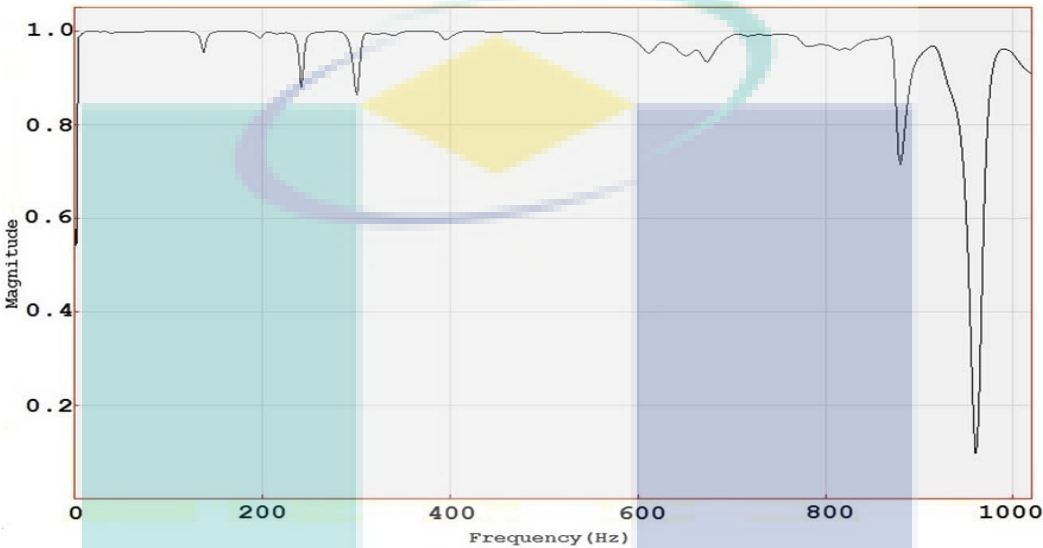


Figure Error! No text of specified style in document..16 Coherence data FRF 3 accelerometers

The value of natural frequencies obtained through curve fitting process in all tests while using 3 accelerometers, including the average for all readings, are exhibited in Table Error! No text of specified style in document..5. According to the table, the nominal value for the natural frequencies obtained when using 3 accelerometers in impact hammer test is more stable compared to the value obtained when using 1 accelerometer. The calculated average reading is used for correlation.

Table Error! No text of specified style in document..5 Experimental natural frequencies of BIW structure when using 3 accelerometers

Mode	Natural frequencies (Hz)				Average
	Roving accelerometer		Roving hammer		
	Reading 1	Reading 2	Reading 1	Reading 2	
1	28.6	28.6	28.8	28.7	28.7
2	45.8	41.5	42.8	42.0	43.0
3	55.1	55.1	59.2	60.0	57.4
4	66.4	66.4	66.6	66.6	66.5
5	70.4	70.8	71.8	71.7	71.2

Meanwhile, while the nominal values of natural frequencies of the BIW structure show diverse reading, the generated mode shapes for every mode remain robust. This indicates that the translation on each point that is measured during testing is stable. The mode shapes for the first, second, third, fourth and fifth mode of the BIW structure are displayed in Figure Error! No text of specified style in document..17.

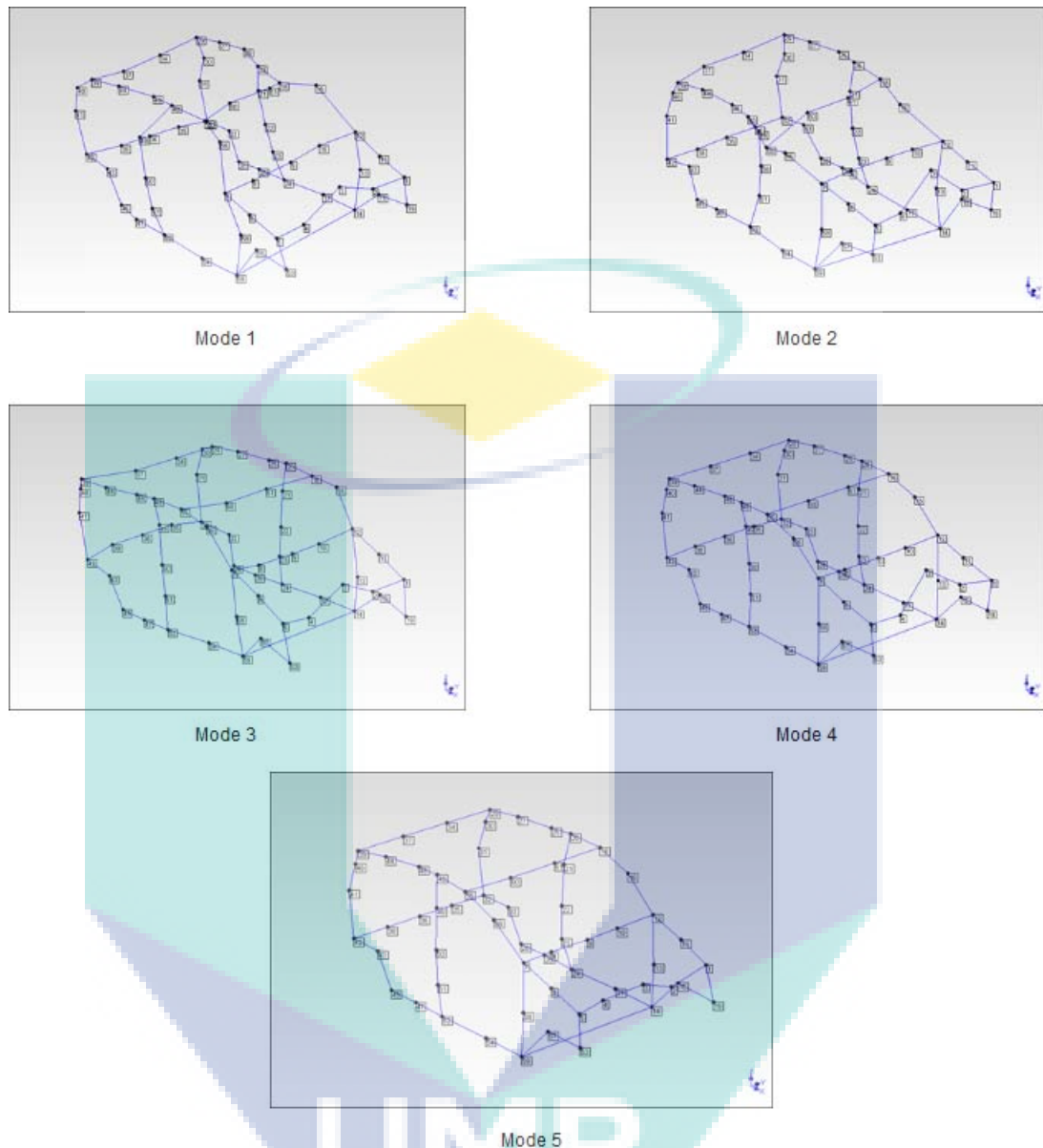


Figure Error! No text of specified style in document..17 Experimental mode shape of BIW structure at each mode

4.4 Finite Element and Experimental Data Correlation

In order to observe how far the results obtained through finite element analysis agree with the one obtained through experimental work; correlation of the gathered modal properties is carried out. The nominal value of the natural frequencies obtained through both finite element and experimental are compared. In furtherance of choosing the better experimental data for further correlation process, the data obtained while using 3 accelerometers for measuring the response from BIW structure is preferred because of the responses obtained when more accelerometers are utilized is more stable and robust. This is decided with reference to the FRF graphs shown in previous section. In Figure Error! No text of specified style in document..14 and Figure Error! No text of specified style in document..15, the peaks that indicate the vibrational modes for the

BIW structure is clearly visible and contain less noise than the FRF graphs shown in Figure Error! No text of specified style in document..7 and Figure Error! No text of specified style in document..8.

With the set of experimental data of the BIW structure available, the validation for the predicted data, which is the finite element data, can be executed. As the experimental modal properties is acknowledged as the actual modal properties of the BIW structure, while the finite element modal data are the predicted data, the correlation of those sets of data can disclose the level of agreement of the different approaches of finite element modelling of BIW to the actual structure. There are three different strategies of modelling the BIW structure in finite element. For each model, the modal properties of the BIW model are extracted using SOL 103 in MSC.Nastran/Patran software. Table Error! No text of specified style in document..6 presents the correlation of experimental and finite element natural frequencies of BIW model with different modelling strategies, which include the BIW model without any joint strategies, and BIW model with joint elements modelled using CBAR and CELAS elements.

Table Error! No text of specified style in document..6 Experimental and finite element natural frequencies of BIW model with different modelling strategies

Mode	Natural frequencies (Hz)						
	Experimental	Finite element (with different modeling strategies)					
		No joint	Error (%)	CBAR joint	Error (%)	CELAS joint	Error (%)
1	28.7	29.37	2.33	29.29	2.06	29.30	2.09
2	43.0	41.30	3.95	43.22	0.51	43.27	0.63
3	57.4	52.55	8.45	55.70	2.96	55.91	2.60
4	66.5	67.15	0.98	62.14	6.56	62.41	6.15
5	71.2	74.59	4.76	69.35	2.60	69.48	2.42
		Average error	4.10	Average error	2.94	Average error	2.78

From the data in Table Error! No text of specified style in document..6, the average error for each mode of the BIW model without joint modelling is 4.10 %, for the BIW model that use CBAR elements for joint modelling is 2.94 %, and for the BIW model that used CELAS elements for joint modelling is 2.78 %. It apparent that BIW model without joint strategies shows higher average error for each mode compared to when joint elements such as CBAR and CELAS are included in the model. Meanwhile, between CBAR and CELAS as joint elements in the BIW model, the average error for each mode does not differ very much which is about 0.16 %. However, numerically, better correlation is achieved while employing CBAR elements to model the joints compared to CELAS elements. Obviously, the results shown in the initial finite element as shown in Table Error! No text of specified style in document..6 can be updated in order to achieve better correlation to the experimental results.

According to Table Error! No text of specified style in document..6, the highest percentage of error is shown by the third mode of BIW model without joint elements which is 8.45%. On the other hand, the highest percentage of error shown by the BIW models with joint elements is found in the fourth mode. In the fourth mode, BIW model with CBAR elements shows 6.56% while BIW model with CELAS elements shows 6.15%. Comparison with other study is made in order to verify the accepted value of error percentage. Sani et al. (2008) in the correlation of dynamic properties of go-kart structure shows the highest error percentage of 33.70%. It was commented that due to the complexity of the model, some simplification on the design was done and resulting the large value of error. In another study carried out by Nehete et al. (2015), the highest percentage of error found in the finite element model of cavities is 15.7%. In a study performed by Husain et al. (2010), the highest initial percentage of error of finite

element model of hat-plate structure is 7.69%. Therefore, for this study, the error found in all model for each mode in study can be considered as acceptable since there are no mode showing error of more than 10%. After all, the constructed finite element models of BIW are the simplified models which are different from its actual counterpart.

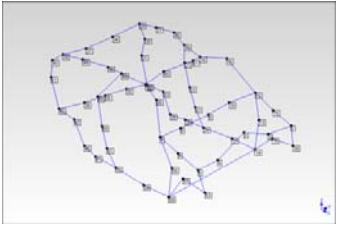
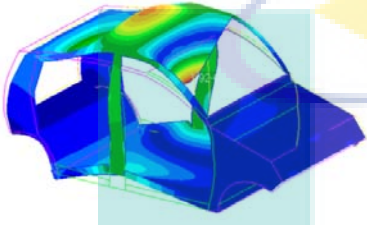
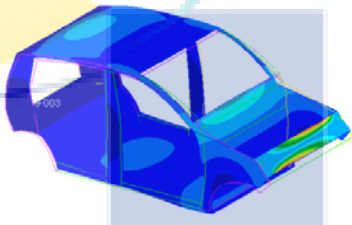
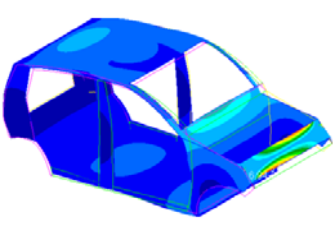
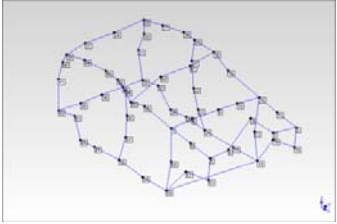
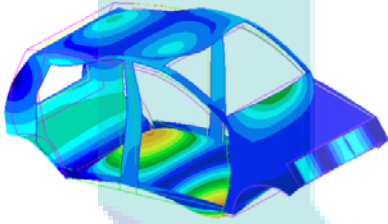
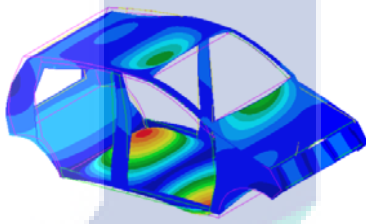
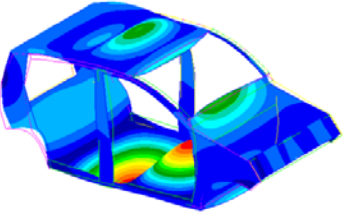
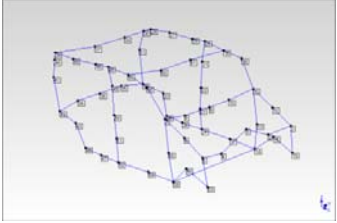
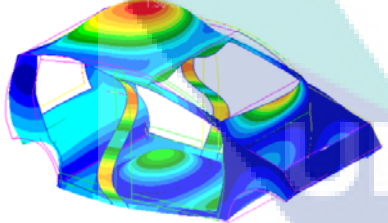
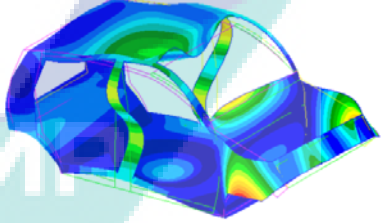
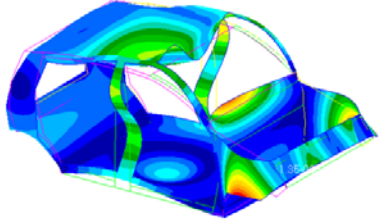
Visual comparison of the experimental mode shapes and the mode shapes obtained in finite element analysis that use different approaches is exhibited in Table Error! **No text of specified style in document..7**. As the experimental mode shapes are displayed through wireframe model rather than the model with surface as viewed by finite element mode shapes, it is harder to make visual comparison with just stationary picture just as shown in Table Error! **No text of specified style in document..7**.

In the first mode, the finite element mode shapes of the BIW model with joint elements are showing bending deformation at floor, roof, body side and front structure area and the amplitude of the movement is lower, while in the finite element mode shape of the BIW model without joint element shows combination of bending and torsional deformation at the roof area and the amplitude of the movement is higher. On the other hand, the experimental mode shape is showing bending movement in each wireframe component. In the second mode, the experimental and all finite element mode shapes are showing similar pattern of deformation even if the direction of bending movement in BIW with CELAS element is differing from others. The same case is shown in the third mode where the finite element mode shape of the BIW model without joint elements is showing the bending motion, though at the same place, but in different direction. In the fourth mode, the deformation shown in finite element mode shape of BIW model with CBAR elements is the same but in opposite direction to the mode shape of the BIW model with CELAS elements. Experimental and finite element mode shape of BIW model without joint elements show similar pattern to the shape shown by BIW model with CELAS elements even if the amplitude of the deformation is different. In the fifth mode, the pattern of all mode shapes shown by all finite element models is in similar pattern, direction and amplitude. However, the experimental mode shape, though shows similar deformation, is deformed in lower amplitude compared to the one shown in finite elements. In addition to this, the results of MAC correlation between the experimental and all the finite element mode shapes are showing the value of more than 80% which indicates that all the modes are well correlated.

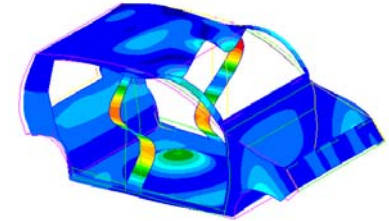
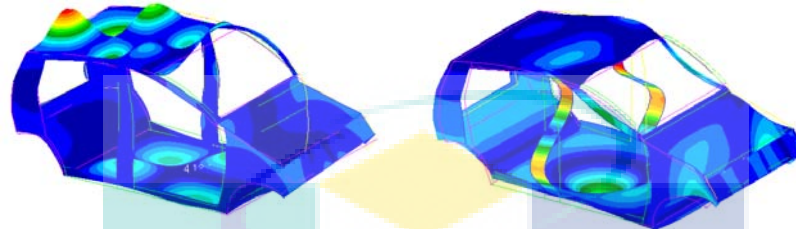
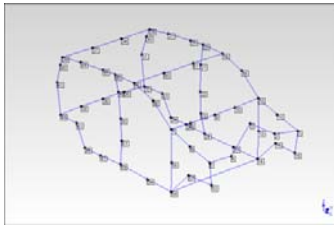
The logo for UMP (Universitas Muhammadiyah Purwokerto) is a large, stylized letter 'M' composed of four triangular segments meeting at the center. The top-left and bottom-right segments are light blue, while the top-right and bottom-left segments are light purple. The letters 'UMP' are printed in white, bold, sans-serif font across the center of the 'M' shape.

UMP

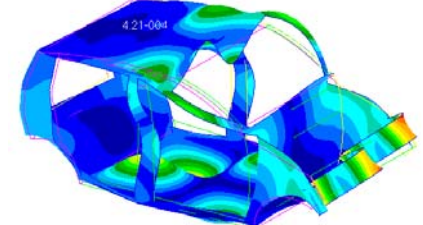
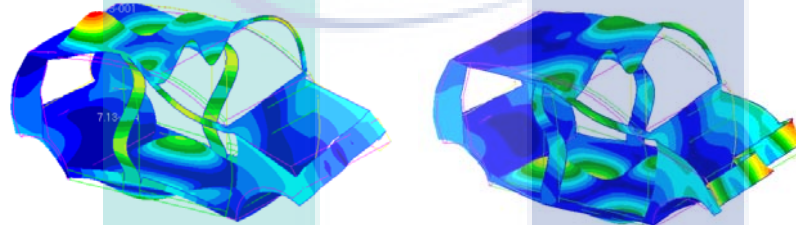
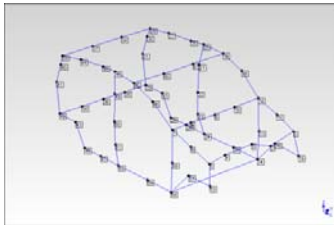
Table Error! No text of specified style in document..7 Experimental and finite element mode shapes of BIW model with different modelling strategies

Mode shapes		Finite element (with different modeling strategies)		
Mode	Experimental	No joint	CBAR	CELAS
1				
2				
3				

4



5



UMP

4.5 Finite Element Model Updating of BIW Structure

Although the results obtained from finite element analysis are sometimes efficient enough to predict the dynamic behaviour of the tested structure, experimental data is always needed in order to validate the predicted data. Consequently, model updating process is essential in order to improve the predicted data so as to represent the actual data more accurately. The parameterization of the finite element model that is using the sensitivity analysis which is based on SOL 200 available in MSC.Nastran/Patran software identifies the sensitive parameters that are selected as the updating parameters.

4.5.1 Updating of the BIW Model without Joint Elements

Based on the sensitivity analysis performed on the selected parameters as described in previous chapter, it appears that Young's modulus and thickness is the most sensitive parameters. Table Error! No text of specified style in document..8 exhibits the sensitivity coefficients of selected updating parameters. According to the data from the sensitivity analysis, from all the thickness parameters included in the analysis, it can be summarized that Thickness 2 is the most sensitive among all. Thickness 4, on the other hand, shows sensitive coefficient for the fourth mode only while Thickness 1 and Thickness 3 is less sensitive for all modes. Some argument can be made that correction of thickness can be performed manually rather than included as an updating parameter. In this case, however, the thickness properties are not only assigned to represent the thickness on the actual structure, but also to replicate the stiffness and rigidity of the surface component. Therefore, the thickness parameter is included as one of the updating parameters so that the suitable value for thickness that should be assigned on the surface so that the rigidity of the surface on the actual structure can be identified and replicated in the finite element model. It also appears that sensitivity coefficient of Young's modulus and density is both showing the same level of sensitivity. However, only one of these two parameters is selected, which is the Young's modulus, as the updating parameter due to their direct relation in the calculation of the natural frequency. In addition, the number of parameters should be kept to be minimum in order to avoid ill-conditioning problem (Husain et al., 2009)

Table Error! No text of specified style in document..8 Sensitivity coefficient for each potential updating parameter of BIW model without joint elements

Parameters	Mode				
	1	2	3	4	5
Young's modulus	1.4372E+01	2.0625E+01	2.6072E+01	3.2056E+01	3.6573E+01
Poisson ratio	6.2252E-01	3.3211E+00	2.9448E-01	5.2410E+00	2.3262E+00
Density	-1.522E+01	-2.185E+01	-2.762E+01	-3.396E+01	-3.874E+01
Thickness 1 (0.001m)	-2.6369E-01	4.3494E+00	-5.3695E-02	6.0279E-02	1.5513E+00
Thickness 2 (0.008m)	1.2588E+01	3.1145E+01	1.7985E+01	1.8180E+00	2.8395E+01
Thickness 3 (0.006m)	5.0923E-01	9.6746E-03	8.8233E-01	4.9524E+00	2.1093E+00
Thickness 4 (0.003m)	2.4575E+00	4.7598E-01	1.5639E-01	5.7903E+01	8.4075E+00

Table **Error! No text of specified style in document..9** shows the updated natural frequencies of the finite element model of BIW without joint elements and comparison of the value from the initial value. Although percentage of error increased after updating in the first and fifth mode, the average error for each mode shown by the updated natural frequencies is decreased by 0.66 %. Moreover, the error shown in the fourth mode is reduced almost to nothing, which is 0.02 %. This is revealing that even if in small percentage value, the simplified finite element model that is modelled by neglecting joint components can still be improved.

Table **Error! No text of specified style in document..9** Comparison of initial and updated finite element natural frequencies of BIW model without joint elements

Mode	Experimental natural frequencies (Hz)	Initial FE natural frequencies with no joint strategies (Hz)	Error (%)	Updated natural frequencies with no joint strategies (Hz)	Error (%)
1	28.70	29.37	2.33	29.43	2.54
2	43.00	41.30	3.95	42.27	1.70
3	57.40	52.55	8.45	53.27	7.20
4	66.50	67.15	0.98	66.51	0.02
5	71.20	74.59	4.76	75.28	5.73
		Average error	4.10	Average error	3.44

The changes of the initial and updated value of the updating parameters which consist of Young's modulus and selected thickness are shown in

Table **Error! No text of specified style in document..10**. The Young's modulus shows an increment of 5.78 % from the initial value while the selected thickness shows the lessening of 5 % and 3.33 % respectively from the initial value. The value of deviation of Young's modulus is greater owing to the reason that the parameter shows higher sensitivity coefficient compared to the thickness during sensitivity analysis. Meanwhile, the initial change of the updating parameters from the initial normalized value until it has achieved a steady value is shown in Figure **Error! No text of specified style in document..18**. Based on the figures, the process of updating becomes complete after 10 iterations for all updating parameters (Young's modulus, Thickness 2 and Thickness 4).

Table **Error! No text of specified style in document..10** Updated value of updating parameter for BIW model without joint elements

Parameters	Initial value, I	Updated value, II	Changes (%)= $ (II-I)/I \times 100$
Young's modulus (GPa)	200	211.56	5.78
Thickness 2 (m)	0.008	0.0084	5.00
Thickness 4 (m)	0.003	0.0029	3.33

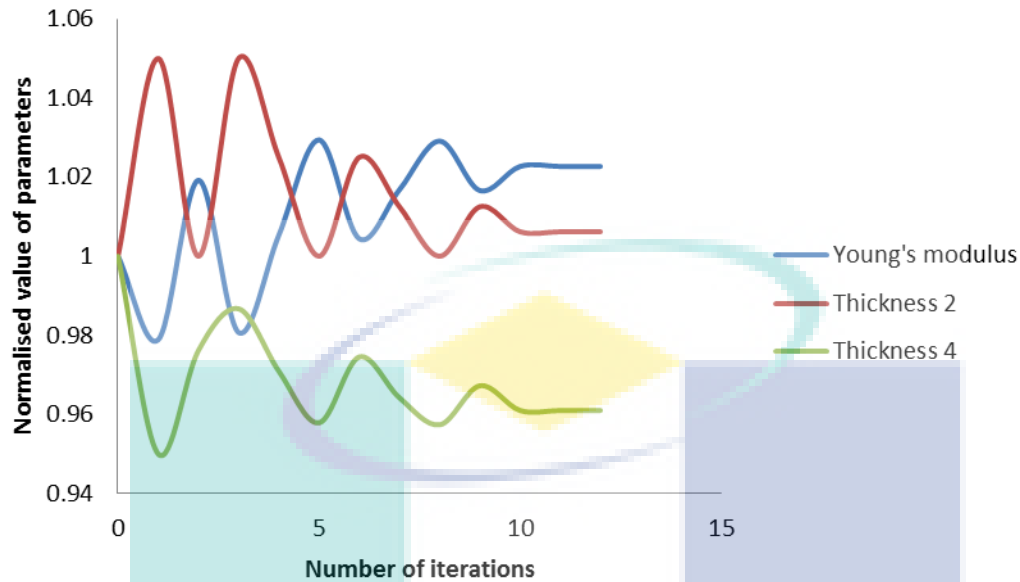


Figure **Error! No text of specified style in document..18** The non-convergence of the updating parameters for BIW model without any joint elements

4.5.2 Updating of the BIW Model with CBAR as Joint Elements

While carrying out sensitivity analysis on the BIW model with joint elements, the parameters of the joint such as the Young's modulus of the connecting elements and the diameter of the beam used for CBAR elements are included as well.

Table **Error! No text of specified style in document..11** provides the outcomes of the sensitivity analysis on the several parameters. The sensitivity coefficients shown in the table indicate that the parameters of the joint elements are less sensitive. Rather, the Young's modulus assigned to the BIW model and the thickness properties are sensitive. For thickness parameters, even if the sensitive coefficient indicates that only certain mode is sensitive to the parameter, the thickness is still selected as one of the updating parameters as it contributes to the mode it sensitive to. In this case, Thickness 2 parameter is sensitive to the fourth mode, Thickness 3 is sensitive to third mode and Thickness 4 is sensitive to the second mode.

Table **Error! No text of specified style in document..11** Sensitivity coefficient for each potential updating parameter of BIW model with CBAR elements

Parameters	Mode				
	1	2	3	4	5
Young's modulus	1.4616E+01	2.1798E+01	2.8345E+01	3.2689E+01	3.6455E+01
Poisson ratio	2.0315E-01	3.5294E+00	2.5162E-01	1.5448E+00	1.4031E+00
Density	-1.342E+01	-2.001E+01	-2.602E+01	-3.000E+01	-3.346E-04
Thickness 1 (0.012m)	-1.536E-01	5.6285E-02	6.6606E-01	5.3006E-01	3.5155E+00
Thickness 2 (0.008m)	6.8212E+00	6.0654E-01	3.7143E+00	3.6428E+01	7.6688E+00
Thickness 3	-8.108E-01	2.973E+00	1.155E+01	1.854E+00	-3.138E-01

(0.006m)					
Thickness 4	-7.065E-01	3.465E+01	2.717E+00	4.201E+00	9.937E+00
(0.003m)					
Beam diameter (m)	4.9403E-08	3.3232E-10	3.3514E-08	1.2452E-08	6.7373E-08
Joint Young's modulus	1.443E-07	7.1838E-10	7.4853E-08	3.7886E-08	1.4664E-07

Table Error! No text of specified style in document..12 exhibits the natural frequencies of the updated BIW model with CBAR joint elements. In this case, the updated value of natural frequency for the first and second mode increased by 1.08 % and 1.77 % respectively from their initial value. However, the average error for each mode for the updated data decreased by 1.2 % from the initial value. In addition, compared to the average error for each mode that is obtained after updating of the BIW model without joint elements as displayed in Table Error! No text of specified style in document..9, the average error for each mode shown by this model is obviously lower.

Table Error! No text of specified style in document..12 Comparison of initial and updated finite element natural frequencies of BIW model with CBAR joint elements

Mode	Experimental natural frequencies (Hz)	Initial FE natural frequencies with CBAR joint (Hz)	Error (%)	Updated natural frequencies with CBAR joint (Hz)	Error (%)
1	28.70	29.29	2.06	29.60	3.14
2	43.00	43.22	0.51	43.98	2.28
3	57.40	55.70	2.96	57.35	0.09
4	66.50	62.14	6.56	65.92	0.87
5	71.20	69.35	2.60	72.85	2.32
		Average error	2.94	Average error	1.74

Meanwhile, the updated value of the chosen updating parameters for the BIW model with CBAR elements are shown in

Table Error! No text of specified style in document..13. The Young's modulus shows the decreased of 7.5 % from the initial value, while the thickness 2 and 3 show higher increment of 25 % and 21.7 % respectively from their initial value. Thickness 4 however, shows only little increment of 3.33 %. Meanwhile, in Figure Error! No text of specified style in document..19, the initial change of the updating parameters from the initial normalized value to convergent value is displayed. The process of updating achieves convergence after 8 iterations for all updating parameters.

Table Error! No text of specified style in document..13 Updated value of updating parameters for BIW model with CBAR elements

Parameters	Initial value	Updated value	Changes (%)= $\frac{ (II-I) }{I} \times 100$
Young's modulus (GPa)	200	185	7.5
Thickness 2 (m)	0.008	0.01	25.00

Thickness 3 (m)	0.006	0.0073	21.67
Thickness 4 (m)	0.003	0.0031	3.33

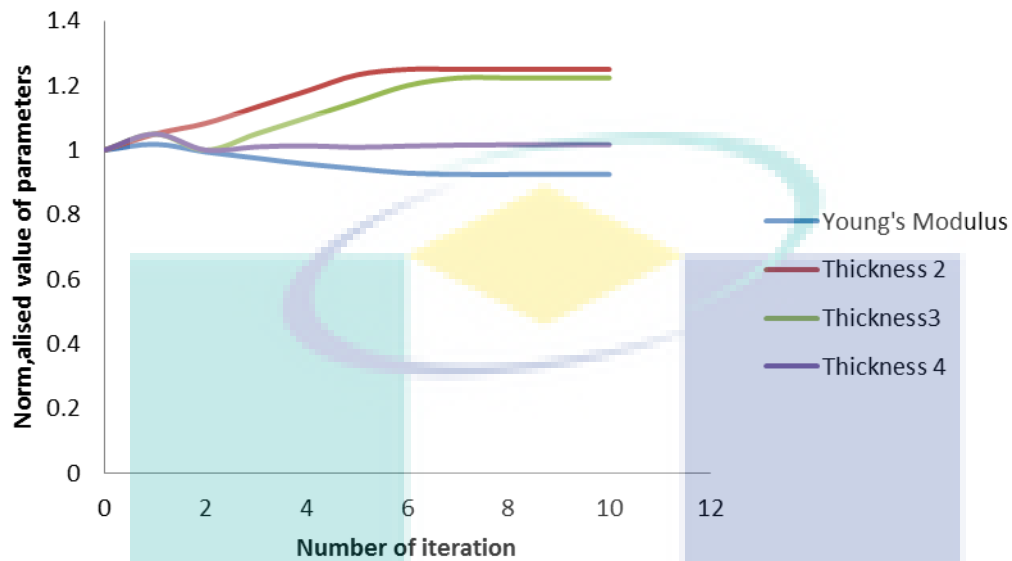


Figure Error! No text of specified style in document..19 The convergence of the updating parameters for BIW model with CBAR elements as joint elements

4.5.3 Updating of the BIW model with CELAS as joint elements

In the sensitivity analysis carried out on the parameters available on the BIW model with CELAS element, the only parameter that can be included for analysis that concerns the properties of joint element is the assigned spring constant. Unlike CBAR element that contains the material and physical properties of the elements, CELAS element only consists of the spring constant value in its element input.

Table Error! No text of specified style in document..14 illustrates the results of the sensitivity analysis on several selected parameters. Similar to the results obtained from model with CBAR elements, the parameter associated with CELAS elements turns out to be not sensitive to be included as one of the updating parameters. Meanwhile, apart from Young's modulus which shows high sensitivity coefficient as shown in the table, several thickness properties, which are Thickness 2, 3 and 4, are selected as the updating parameter. Similar to previous cases that are described in previous subsection, the thicknesses are not showing satisfactory sensitivity coefficient for all modes in study. However, Thickness 2 shows high sensitivity towards the fourth mode, Thickness 3 shows high sensitivity towards the third mode, and Thickness 4 shows high sensitivity towards the second mode. It is due to this situation that the thickness properties are included as updating parameters.

Table Error! No text of specified style in document..14 Sensitivity coefficient for each potential updating parameter of BIW model with CELAS elements

Parameters	Mode				
	1	2	3	4	5
Young's modulus	1.7242E+01	2.5764E+01	3.3546E+01	3.8597E+01	4.3234E+01
Poisson ratio	2.0919E-01	3.5227E+00	2.6779E-01	1.5809E+00	1.2860E+00

Density		-1.578E+01	-2.357E+01	-3.072E+01	-3.541E+01	-3959E+01
Thickness (0.012m)	1	-1.282E-01	4.802E-02	4.642E-01	5.893E-01	3.4477E+00
Thickness (0.008m)	2	6.8693E+00	5.8854E-01	3.6417E+00	3.5389E+01	8.0408E+00
Thicknes (0.006m)	3	-8.221E-01	2.9712E+00	1.1916E+01	1.6767E+00	2.4106E-02
Thickness (0.003m)	4	-7.020E-01	3.4650E+01	2.3123E+00	3.7314E+00	9.2612E+00
Spring constant		8.2102E-03	4.5076E-04	2.4698E-02	8.5638E-02	2.9939E-02

Table **Error! No text of specified style in document..15** displays the natural frequencies of the updated BIW model with CELAS joint elements. In this case, only the first and second mode is showing the increase of natural frequencies value after updating. For the first mode, the natural frequency value increased by 1.01 % from its initial value while for the second mode, the value of natural frequency increased by 1.72 % from its initial value. The average error for each mode after updating is reduced by about 1.05 % from the initial value of average error for each mode.

Table **Error! No text of specified style in document..15** Comparison of initial and updated finite element natural frequencies of BIW model with CELAS elements

Mode	Experimental natural frequencies (Hz)	Initial natural frequencies with CELAS joint (Hz)	FE Error (%)	Updated natural frequencies with CELAS joint (Hz)	Error (%)
1	28.70	29.30	2.09	29.59	3.10
2	43.00	43.27	0.63	44.01	2.35
3	57.40	55.91	2.60	57.38	0.03
4	66.50	62.41	6.15	65.96	0.81
5	71.20	69.48	2.42	72.87	2.35
		Average error	2.78	Average error	1.73

Next, the updated value of the chosen updating parameters for the BIW model with CELAS elements are shown in

Table **Error! No text of specified style in document..16**. The updated value of Young's modulus lessens by 7.58 %. Other updating parameters however, are showing the exact increment as the updated value of model with CBAR elements as shown in Table **Error! No text of specified style in document..13**. Meanwhile, Figure **Error! No text of specified style in document..20** shows the initial change of the updating parameters from the initial normalized value to convergent value. The process of updating achieves convergence after 8 iterations.

Table **Error! No text of specified style in document..16** Updated value of updating parameter for BIW model with CELAS elements

Parameters	Initial value	Updated value	Changes (%)= $\frac{ (I-I) }{I} \times 100$
------------	---------------	---------------	--

Young's modulus (GPa)	200	184.84	7.58
Thickness 2 (m)	0.008	0.01	25.00
Thickness 3 (m)	0.006	0.0073	21.67
Thickness 4 (m)	0.003	0.0031	3.33

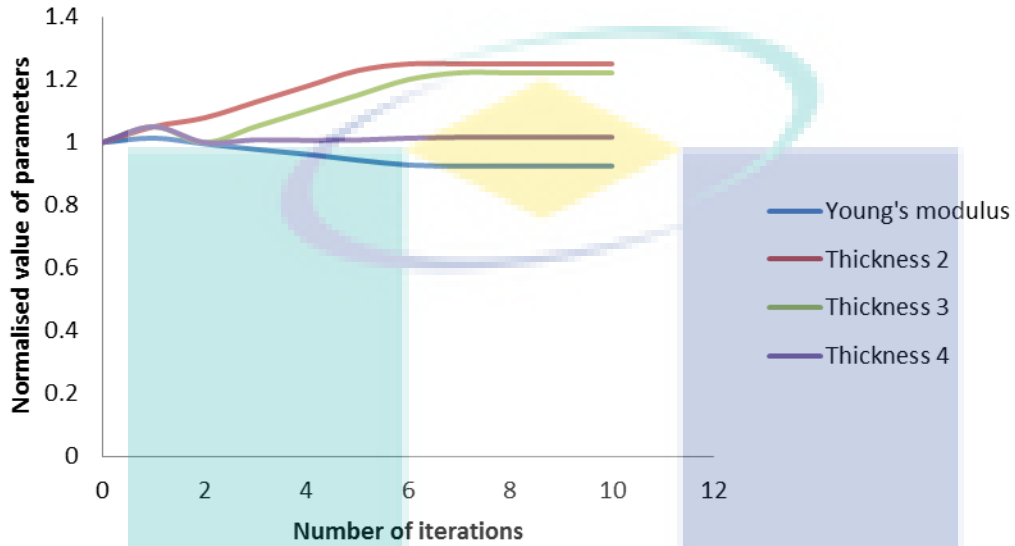


Figure Error! No text of specified style in document..20 The convergence of the updating parameters for BIW model with CELAS elements as joint elements

The equations of motion of discretised structures in the physical space can be expressed as

$$M\ddot{x} + C\dot{x} + Kx + g_{nl}(x, \dot{x}) = f(t) \quad (\text{Eq 1})$$

where M , C and K are $n \times n$ mass, damping and stiffness matrices; g_{nl} is an $n \times n$ nonlinear stiffness matrix, $f(t)$ is applied nodal force vector and $x(t)$ is the vector of physical displacements. The equations can be obtained for example, from finite element modelling of a structure. Transformation by $x = \Phi p$ leads to

$$\Phi^T M \Phi \ddot{p} + \Phi^T C \Phi \dot{p} + \Phi^T K \Phi p + \Phi^T g_{nl}(\Phi p) = \Phi^T f(t) \quad (\text{Eq 2})$$

where Φ is the modal vector matrix. By using orthogonality of the modes, equation (2) become

$$M_p \ddot{p} + C_p \dot{p} + K_p p + \bar{g}_{nl} = \bar{f} \quad (\text{Eq3})$$

where $M = \Phi^T M \Phi = [M_{rr}]$ and $K = \Phi^T K \Phi = [K_{rr}]$ are diagonal matrices, and $\bar{g}_{nl} = \Phi^T g_{nl}$. If the structure has proportional damping, $C = \Phi^T C \Phi = [C_{rr}]$ is also a diagonal matrix and equation (3) reduces to

$$M_{rr} \ddot{p}_r + C_{rr} \dot{p}_r + K_{rr} p_r + \bar{g}_{nl,r} = \bar{f}_r \quad (\text{Eq 4})$$

where ϕ_r is the r th modal displacement and other parameters in modal expression. Nonlinear terms, F_{nlr} refer to r th mode nonlinear restoring force and others mode allow for nonlinear cross-coupling terms.

5. CONCLUSION

A nonlinear simple structure was identified using the force appropriation and restoring forces method. Algorithm has been developed for multiple degree of freedom. Finite element model of BIW has been developed in MSC Nastran Patran and run for normal mode analysis in order to determine modal properties such as natural frequency, mode shape and damping ratio.

The aim of this work is to develop nonlinear identification method of BIW structure. Force appropriation method is developed to excite single mode of structure by applying multiple forces. If the response of the system could be reduced to that of the mode of interest, then a single degree of freedom restoring force identification could be performed to identify any nonlinearity present. Beside of that several method of modal testing are used such as impact hammer, single shaker (spectral test), double shaker (spectral test), MIMO sine testing and MIMO normal mode were carried out to obtain dynamics properties and other parameters. Finite element modelling and model updating was applied to minimise the discrepancies between numerical and experimental dynamic result. As conclusion, this thesis covered numerical works (finite element), experimental works and programming works (matlab coding) to present the nonlinear identification method of the engineering structure.

ACHIEVEMENT

- i) Name of articles/ manuscripts/ books published
 - a) Car Body In White (BIW), Article in Auto Inexss, Automotive Engineering Centre, Issue 9:2015, Universiti Malaysia Pahang
- ii) Title of Journal/Conference Paper presentations (international/ local)
 - a) Force Appropriation Method for Two Degree of Freedom Nonlinear System, Jurnal Teknologi (Sciences and Engineering), Vol. 76 (8), 2015, pp 5-9, ISSN (online): 2180-3722, (Scopus Indexing)
 - b) A Review on Model Updating In Structural Dynamics, Materials Science and Engineering100 (2015) 012015 doi:10.1088/1757-899X/100/1/012015 (Scopus Indexing)
 - c) Dynamics properties of a Go-kart chassis structure and its prediction improvement using model updating approach", International Journal of Automotive and Mechanical Engineering (IJAME), Vol. 14, pg 3887-3897, 2017, doi: <https://doi.org/10.15282/ijame.14.1.2017.6.0316> (Scopus Indexing)
 - d) Correlation of numerical and experimental analysis for dynamic behavior of a Body-In-White (BIW) structure", Journal MATEC of Conference, 90 (01020), 2017, pp 1-10, doi: 10.1051/matecconf/20179001020 (Scopus Indexing)
 - e) Correlation of Structural Modal Properties of Go-kart Frame Structure between Different Joint Finite Element Modeling Strategy and Modal Testing - International Conference on Computational Science and Engineering (ICSSE), 20-30 Nov 2016. (will publish in scopus: Advanced Science Letter)

- iii) Human Capital Development
 - a) Master Student:
 - i) Noor Am Zura Abdullah - MMA14003
 - ii) Khaironi Mat Jelani – MMA16003
 - b) Undergraduate Student
 - i) Muhamad Shukri Aimi Abd. Aziz - MA10039
 - ii) Muhammad Hafiz Esa - MA10122
 - iii) Nur Syafenazzatul Ain Mat Saad - MA11082
 - iv) Ibnu Abbas Othman - MA12051
 - v) Matheus Anak Johani - MA12089
- iv) Awards/ Others
- v) Others

REFERENCES

- [1] K. Worden, and G. R. Tomlinson, "Nonlinearity in structural dynamics: Detection, identification and modelling", University of Sheffield: Institute of Physics Publishing, (2001)
- [2] N. M. M. Maia, and J. M. M. Silva, "Theoretical and experimental modal analysis", Research Studies Press, Taunton, (1997)
- [3] D. J. Ewins, "Modal testing: theory and practice", Research Studies Press, Letchworth, (1995)
- [4] R. K. Dearson, "Discrete time dynamic model", Oxford University Press, (1994)
- [5] Ö. Arslan, M. Aykan, H. N. Özgüven, "Parametric identification of structural nonlinearities from measured frequency data", Mechanical System and Signal Processing, vol. 25 , no. 11, pp 1112-1125, (2011)
- [6] G. Kerschen, K. Worden, A. F. Vakakis and J.C. Golinval, "Past, present and future of nonlinear system identification in structural dynamics", Mechanical System and Signal Processing, vol. 20 , pp 505-592, (2006)
- [7] A. Hot, G. Kerschen, E. Foltête and S. Cogan, "Detection and quantification of non-linear structural behavior using principal component analysis", Mechanical System and Signal Processing, vol. 26, 104-116, (2012)
- [8] S. F. Masri, and T. K. Caughey, "A nonparametric identification technique for nonlinear dynamic problems", Journal of Applied Mechanics, vol. 46, pp. 433-447, (1979)
- [9] S. F. Masri, H. Sassi, and T. K. Caughey, "Nonparametric identification of nearly arbitrary nonlinear systems", Journal of Applied Mechanics, vol. 49, pp. 619-628,(1982)
- [10] E. F. Crawley, and A. C. Aubert, "Identification of nonlinear structural elements by force-state mapping", AIAA Journal, vol. 24, pp. 155-162, (1986)
- [11] G. Dimitriadis, and J. E. Cooper, "A method for the identification of non-linear multi-degree-of-freedom systems", Proceedings of the Institute of Mechanical Engineers, Part G 212, pp. 287-298, (1998)

- [12] G. Kerschen, J. C. Golinval and K. Worden, "Theoretical and experimental identification of a non-linear beam", *Journal of Sound and Vibration*, vol. 244, pp. 597-613, (2001)
- [13] M. Aykan, and H. N. Özgüven, "Parametric identification of nonlinearity from incomplete FRF data using describing function inversion", In: *Proceedings of the SEM IMAC XXX conference*, Jacksonville, vol 3, (2012)
- [14] M. Aykan, and H. N. Özgüven, "Identification of restoring force surfaces in Nonlinear MDOF systems from FRF data using nonlinearity matrix", *Conference Proceedings of the Society for Experimental Mechanics Series*, vol. 35, pp 65-76, (2013)
- [15] M.S.M. Sani, H. Ouyang, J.E. Cooper and C.K.E.N.C.K. Husin, "Smart Methodology of Stiffness Nonlinearity Identification Vibration System", *2nd International Conference on Mechanical Engineering Research 2013 (ICMER)* (2013)
- [16] J. P. Noel, G. Kerschen, and A. Newerla, "Application of the Restoring Force Surface Method to a Real-life Spacecraft Structure", *Conference Proceedings of the Society for Experimental Mechanics Series*, pp 1-19, (2012)
- [17] O. Arslan (2008). *Modal identification of nonlinear substructures and implementation in structural coupling analysis*, M.Sc. Thesis, Department of Mechanical Engineering, Middle East Technical University, Ankara, Turkey.
- [18] G. Kerschen (2002). *On the model validation in non-linear structural dynamics*. PhD Thesis, Department of Aeronautical, University of Liege, Belgium.
- [19] P.J. Roache (1998). *Verification and Validation in Computational Science and Engineering*, Hermosa Publications, Albuquerque.
- [20] G. Kerschen, K. Worden, A.F. Vakakis and J. C. Golinval (2006). Past, present and future of nonlinear system identification in structural dynamics, *Mechanical Systems and Signal Processing*, vol. 20, no. 3, pp 505-592.
- [21] P. Ibanez (1976). Force appropriation by Extended Asher's method. *SAE Aerospace Engineering and Manufacturing Meeting*, SAE Paper, no.760873.
- [22] S.F. Masri and T.K. Caughey (1979). A nonparametric identification technique for nonlinear dynamic problems. *Journal of Applied Mechanics*, vol. 46, pp. 433-447
- [23] S.F. Masri, H. Sassi and T.K. Caughey (1982). Nonparametric identification of nearly arbitrary nonlinear systems. *Journal of Applied Mechanics*, vol. 49, pp. 619-628
- [24] E.F. Crawley and A.C. Aubert (1986). Identification of nonlinear structural elements by force-state mapping. *AIAA Journal*, vol. 24, pp. 155-162
- [25] G. Dimitriadis and J.E. Cooper (1998). A method for the identification of non-linear multi-degree-of-freedom systems. *Proceedings of the Institute of Mechanical Engineers*, Part G 212, pp. 287-298.
- [26] G. Kerschen, J. C. Golinval and K. Worden (2001). Theoretical and experimental identification of a non-linear beam. *Journal of Sound and Vibration*, vol. 244, pp. 597-613.
- [27] M. Simon and G. R. Tomlinson (1984). Use of the Hilbert transform in modal analysis of linear and non-linear structures. *Journal of Sound and Vibration*, vol. 96, pp. 421-436.
- [28] G. R. Tomlinson (1987). Developments in the use of the Hilbert transform for detecting and quantifying non-linearity associated with frequency response functions. *Mechanical Systems and Signal Processing*, vol. 1, no. 2, pp. 151-171.
- [29] M. Feldman (2007). Considering high harmonics for identification of non-linear systems by Hilbert transform. *Mechanical System and Signal Processing*, vol. 21, no. 2, pp 943-958.
- [30] J. S. Bendat (1990). *Nonlinear system analysis and identification from random data*. John Wiley & Sons. New York, U.S.A.

- [31] H. J. Rice and J.A. Fitzpatrick (1991). A procedure for the identification of linear and non-linear multi-degree-of freedom systems. *Journal of Sound and Vibration*, vol. 149, pp. 397-411.
- [32] C. M. Richards and R. Singh (1998). Identification of multi-degree-of-freedom non-linear systems under random excitations by the reverse-path spectral method. *Journal of Sound and Vibration*, vol. 213, pp. 673-708.
- [33] S. Marchesiello (2003). Application of the conditioned reverse path method, *Mechanical Systems and Signal Processing*, vol. 17, pp. 183-188.
- [34] R. M. Lin, D. J. Ewins and M. K. Lim (1993). Identification of nonlinearity from analysis of complex modes. *International Journal of Analytical and Experimental Modal Analysis*, vol. 8, no. 3, pp. 290-306.
- [35] H. R. E. Siller (2004). *Nonlinear modal analysis methods for engineering structures*. PhD Thesis, Department of Mechanical Engineering, Imperial College London, UK.
- [36] P. M. Slaats, J. De Jongh and A. A. H. J. Sauren (1995). Model reduction tools for nonlinear structural dynamics. *Computers & structures*, vol. 54, no. 6, pp. 1155-1171.
- [37] S. W. Shaw and C. Pierre (1991). Normal modes for nonlinear vibratory systems. *Journal of Sound and Vibration*, vol. 164, no. 1, pp. 85-124.
- [38] N. Boivin, C. Pierre and S. W. Shaw (1995). Nonlinear modal analysis of structural systems featuring internal resonances. *Journal of Sound and Vibration*, vol. 182 no. 2, pp. 225-230.
- [39] E. Pesheck, N.Boivin and C. Pierre (2001). Nonlinear modal analysis of structural systems using multi-mode invariant manifolds. *Nonlinear Dynamics*, vol. 25, pp. 183-205.
- [40] H. J. Rice (1995). Identification of weakly nonlinear systems using equivalent linearization. *Journal of Sound and Vibration*, vol. 185, no. 3, pp. 473-481.
- [41] C. Soize and O. Le Fur (1997). Modal identification of weakly nonlinear, multidimensional dynamical systems using a stochastic linearisation method with random coefficients. *Mechanical Systems and Signal Processing*, vol. 11, no. 1, pp. 37-49.
- [42] L. F. Rosa, C. Magluta and N. Roitman (1999). Estimation of modal parameters through a nonlinear optimisation technique. *Mechanical Systems and Signal Processing*, vol. 13, no. 4, pp. 593-607.
- [43] M. A. Al-Hadid and J. R. Wright (1989). Developments in the force-state mapping technique for non-linear systems and the extension to the location of nonlinear elements in a lumped-parameter system. *Mechanical Systems and Signal Processing*, vol. 3, no. 3, pp. 269-290.
- [44] M. I. McEwan, J. R. Wright, J. E. Cooper and A. Y. T. Leung (2001). A combined modal/finite element analysis technique for the dynamic response of a nonlinear beam to harmonic excitation. *Journal of Sound and Vibration*, vol. 243, pp. 601-624.
- [45] I. J. Leontaritis and S. A. Billings (1985). Input-output parametric models for nonlinear systems, part I: deterministic nonlinear systems, vol. 41, pp. 303-328.
- [46] F. Thouverez and L. Jezequel (1996). Identification of NARMAX models on a modal base. *Journal of Sound and Vibration*, vol. 89, pp. 193-213.
- [47] S. Billings, S. Chen, and M. Korenberg (1989). Identification of MIMO nonlinear systems using a forward regression orthogonal estimator. *International Journal of Control*, vol. 49, no. 6, pp. 2157-2189.
- [48] Q. Chen, K. Worden, P. Peng and A. Leung (2007). Genetic algorithm with an improved fitness function for NARMAX modelling. *Mechanical Systems and Signal Processing*, vol. 21, no. 2, pp. 994-1007.

APPENDIXES

